Journal of Alloys and Compounds 509 (2011) 8952–8957

Contents lists available at ScienceDirect

Journal of Alloys and Compounds

journal homepage: www.elsevier.com/locate/jallcom

The magnetic, structure and mechanical properties of rapidly solidified $(Nd_7Y_{2.5})$–$(Fe_{64.5}Nb_3)$–B_{23} nanocomposite permanent magnet

Zubair Ahmad, Shan Tao, Tianyu Ma, Guoliang Zhao, Mi Yan*

State Key Laboratory of Silicon Materials, Department of Materials Science and Engineering, Zhejiang University, Hangzhou 312007, China

ARTICLE INFO

Article history:
Received 29 May 2011
Received in revised form 15 June 2011
Accepted 16 June 2011
Available online 28 June 2011

Keywords:
Nanocomposite magnet
Magnetic properties
Mechanical properties
Permanent magnet

ABSTRACT

The $Nd_7Y_{2.5}Fe_{64.5}Nb_3B_{23}$ nanocomposite permanent magnets in the form of rods with 2 mm in diameter have been developed by annealing the amorphous precursors produced by copper mold casting technique. The phase evolution, structure, magnetic and mechanical properties were investigated with X-ray diffractometry, differential scanning calorimetry, electron microscopy, magnetometry and universal uniaxial compression strength techniques. The heat treatment conditions under which the magnets attained maximum magnetic and mechanical properties have been established. The results indicate that magnet properties are sensitive to grain size and volume content of the magnetic phases present in the microstructure. The composite microstructure was mainly composed of soft α-Fe (20–30 nm) and hard $Nd_2Fe_{14}B$ (45–65 nm) magnetic phase grains. The maximum coercivity of 959.18 kA/m was achieved with the magnets annealed at 760 °C whereas the highest remanence of 0.57 T was obtained with the magnets treated at 710 °C. The optimally annealed magnets possessed promising magnetic properties such as ${}_jH_c$ of 891.52 kA/m, B_r of 0.57 T, $M_r/M_s = 0.68$, $(BH)_{max}$ of 56.8 kJ/m^3 as well as the micro-Vickers hardness (H_v) of 1138 ± 20 and compressive stress (σ_f) of 239 ± 10 MPa.

1. Introduction

The rapidly solidified nanocomposite permanent magnets consisting of a fine mixture of hard $(Nd,Pr)_2Fe_{14}B$ (to provide coercivity) and soft α-Fe or Fe_3B (to provide magnetization) phases have attracted much scientific and technological interest for the development of the next generation permanent magnets [1,2]. The compositional modification and process optimization approaches have been employed to improve glass forming ability, structure and magnetic properties with $(Nd, Pr)_{3–9.5}$–Fe_{bal}–$M_{2–5}$–$B_{6–30}$; (M = Co, Mo, Nb, Ti, V, Zr) alloy systems [3–6]. The bulk nanocomposite permanent magnets in the rods form with 0.5–1.2 mm in diameter have been successfully developed by copper mold casting technique either in direct casting state or annealing the amorphous precursors [7–10]. The conventional way to develop a permanent magnet through copper mold casting is to make the amorphous alloy and then annealing it at 600–700 °C for 10–30 min. These magnets have the advantages over sintered magnets due to lower raw materials cost, isotropic and in some cases with higher energy products, easier to magnetize in any direction, less contamination or forming oxides due to short processing cycle and higher corrosion resistance due to involvement of lower rare earth (RE) content. A maximum energy product of 400 kJ/m^3 has been predicted for the isotropic nanocomposite magnets by micromagnetic calculations [11], but so for energy product in the range of 80–160 kJ/m^3 [12–16] has been achieved. This discrepancy is attributed to the difficulty in obtaining optimized microstructure containing nanoscale phase grains with homogenous grains distribution. It was found that the hard magnetic performance of nanocomposites can be improved by refining the microstructure, in particular the magnetic properties of the constituent phases.

Recent studies indicate that micro- and macro-additions of Nb [17], Zr [10], Ti [18], Mo [19] to α-Fe or $Fe_3B/Nd_2Fe_{14}B$ type nanocomposite permanent magnets have played the effective and important roles in improving the glass forming ability, refining the phase grains, suppressing the nonmagnetic phases, assisting the formation of desired magnetic phases and controlling the kinetics of crystallization. Similarly, the contents of Nd [20,21] and Y [22] have remarkable effects on the phase formation as well as glass forming ability of the nanocomposite magnets. An important suggestion follows that the effects of these additives are phase selective. Therefore, it might be possible to improve and even tune the structural, magnetic, and mechanical properties of the nanocomposite permanent magnets by controlling and adjusting the contents of alloy constituents [23].

Zhang et al. [17] reported that after optimal crystallization, the bulk $Nd_{9.5}Fe_{bal}Nb_4B_{22.08}$ alloy shows large intrinsic coercivity of 1098.5 kA/m and $(BH)_{max} = 31.8$ kJ/m^3. It was found that

* Corresponding author. Tel.: +86 571 8795 2730; fax: +86 571 8795 2366.
E-mail address: mse_yanmi@zju.edu.cn (M. Yan).

0925-8388/$ – see front matter © 2011 Elsevier B.V. All rights reserved.
doi:10.1016/j.jallcom.2011.06.092

Nb significantly improves the glass forming ability, refine the microstructure and increases the coercivities. However, $(BH)_{max}$ was lower due to low remanence and the existence of a considerable volume fraction of the magnetically soft Fe_3B and/or α-Fe phases. It was also pointed out that Y element is effective in improving glass forming ability, stabilizing the amorphous phase, reducing oxides during melting or heat treatment especially in low purity alloy and improving remanence [22]. Tan et al. [10] also developed $Nd_5Y_4Fe_{68}Zr_2B_{21}$ bulk sheet specimens with relatively larger size of 0.8 mm × 10 mm × 50 mm, which after crystallization at 690 °C exhibit permanent magnetic properties of ${}_jH_c$ = 382 kA/m and $(BH)_{max}$ = 42.9 kJ/m^3. Although the magnetic product was obtained in large size but it possesses low magnetic properties. The lower magnetic properties in these sheets magnets were attributed to the formation of the non-ferromagnetic $NdFe_4B_4$ and $NdFe_3B_3$ phases as well as lower remanence.

For the rapidly solidified nanocomposite permanent magnets, it has been desirable to obtain large size rods (rod >1.2 mm in diameter) with better magnetic properties to extend their industrial applicability. The present study aims to develop macroscopically large size bulk nanocomposite $Nd_7Y_{2.5}Fe_{64.5}Nb_3B_{23}$ permanent magnet in the form of rods and to investigate the structural, magnetic and mechanical properties which would shed some lights on the future design of the bulk nanocomposite magnets for scientific inquiry and industrial applications. The mechanical properties for the rapidly solidified nanocomposite permanent magnets were studied first time in the present alloy system. For the present work, the $Nd_7Y_{2.5}Fe_{64.5}Nb_3B_{23}$ alloy was selected based on our previous studies [19] and considering the thermodynamic empirical rules reported in Refs. [24,25].

2. Experimental

Cast ingots with nominal composition $Nd_7Y_{2.5}Fe_{64.5}Nb_3B_{23}$ were obtained by arc melting the metals Fe, Nd, Y, Nb, and Fe–B alloy (Fe 99.5, Nd, Nb, Y, FeB 99.9% pure) under high purity Ar atmosphere. The ingots were remelted six times to ensure homogeneity. Amorphous rods of 2 mm in diameter and 32 mm in length were prepared by injection copper mold casting technique. The glass transition and crystallization temperature of the amorphous phase was measured using a differential scanning calorimetry (DSC, NETZSCH DSC 404 C) at a constant heating rate of 5 °C/min. The samples were annealed in the temperature range of 660–810 °C for 15 min under protective Ar atmosphere.

The crystalline structure was determined by X-ray diffraction technique with Cu K_α radiation (XRD, PANalytical X'Pert Pro). For peak resolution, each X-ray diffraction pattern was measured in the interval of $20^\circ < 2\theta < 100^\circ$, using the scan speed of 0.5°/min and step size of 0.002°. The phases observed in the X-ray diffraction patterns were identified by comparing the observed peak positions (2θ) and their corresponding intensities (I) with the standard powder diffraction files (PDF) using the Hanawalt method [26]. The mean crystallite sizes of the phases were evaluated by the X-ray diffraction method using the Scherrer's equation [27] by taking into account non-overlapped diffraction peaks corresponding to main $Nd_2Fe_{14}B$ and α-Fe phases.

The density of the magnetic samples was measured using Archimedes principle. The uniaxial compressive tests on the cylindrical rods were performed with a universal testing machine (CMT5205 SANS, China) at a deformation rate of 5×10^{-4} s^{-1}. The tested samples with 2 mm in diameter and 4 mm in length were obtained from the as-cast rods and four samples were tested to ensure the reliability of the results in each case. Vickers hardness (H_v) measurements were conducted using an MVK-E micro-Vickers hardness tester with the load and the dwelling time of 200 g and 15 s, respectively. For the better statistical hardness data, at least 15 measurements were performed for each sample. Microstructural studies were investigated using a high resolution scanning electron microscope (HRSEM, Hitachi S-4800) and high resolution transmission electron microscope (HRTEM, JEOL JEM 2010). The phase compositions in the nanocomposites were determined by energy dispersive spectroscopy (EDS) analysis. For HRSEM examination, longitudinal samples of the as-cast rods were etched in 3% nital solution after polishing down to 0.5 μm finish using a diamond paste. The longitudinal samples were prepared from the outer surface of the as-cast rod i.e., the surface close to casting mold wall referred as peripheral sample and from the inner surface i.e., half-cut along the rod axis referred as a core sample. The magnetic properties were measured at room temperature by using a Quantum Design MPMS-75 superconducting quantum interference device (SQUID) with a maximum applied field of 5 T after the calibration with a standard sample.

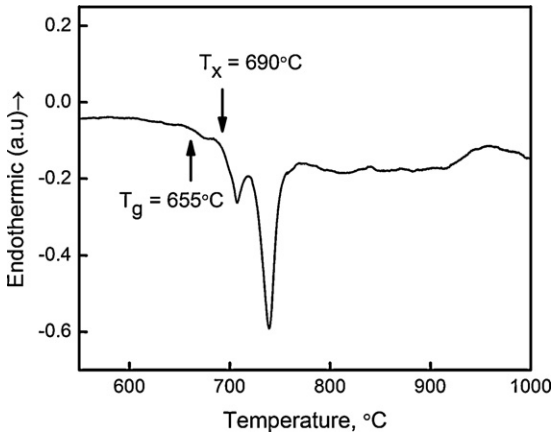

Fig. 1. DSC profile of the as-cast rod of 2 mm in diameter.

3. Results and discussion

Fig. 1 shows the DSC curve for the as-cast alloy. As seen, the curve shows two crystallization temperatures located at about 690 °C and 720 °C, respectively. The X-ray diffraction pattern and outer surface appearance of the as-cast rods are presented in Fig. 2. The X-ray diffraction studies reveal a broad peak or no crystalline peak indicating that as-cast rod was amorphous within the detection limit of X-ray diffraction technique (Fig. 2a). As seen in Fig. 2b, the as-cast rod shows a metallic luster surface, 2 mm in diameter and 32 mm in length. The HRSEM images of the peripheral and core samples for the as-cast rod are presented in Fig. 3. The SEM image shows

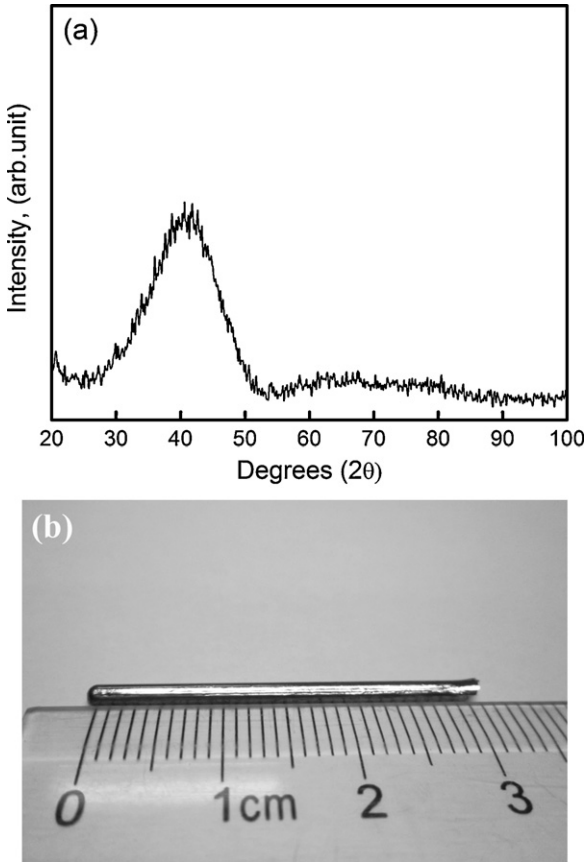

Fig. 2. The X-ray-diffraction pattern (a) and (b) physical surface appearance of as-cast rod.

featureless structure for the peripheral sample (Fig. 3a), while the core sample shows a little amount of crystalline phase (bright spots) in the amorphous matrix (Fig. 3b). The EDS analysis confirmed that bright spots are enriched with Fe element. This result indicates that bright spots might be α-Fe or Fe_3B phase [28], suggesting that core of the as-cast rod was partly crystallized due to slow cooling rate as compared one with peripheral sample.

Fig. 4 shows the X-ray diffraction patterns of the annealed magnets at 660, 710 and 760 °C for 15 min, respectively. The crystalline peaks in the XRD patterns were indexed to the soft α-Fe, Fe_2Nb, Fe_3B, $Nd_2Fe_{23}B_3$ magnetic phases and the hard $Nd_2Fe_{14}B$ magnetic phase. Annealing at 660 °C shows a dual phase structure i.e., crystalline phase and residual amorphous phase. It is obvious due to incomplete crystallization, as the selected annealing temperature is not appropriate to transform the amorphous phase completely into crystalline phase. Thus, high temperature annealing is essential to complete the crystallization. Annealing at 710 °C shows the quaternary-phase nanostructure corresponding to the α-Fe, Fe_2Nb, Fe_3B, $Nd_2Fe_{23}B_3$ and $Nd_2Fe_{14}B$ phases. The mean crystallite sizes at 710 °C for the α-Fe and $Nd_2Fe_{14}B$ phases were measured as 24.7 nm and 49.2 nm, respectively. When annealed at 760 °C, the same α-Fe, Fe_2Nb, Fe_3B, $Nd_2Fe_{23}B_3$ and $Nd_2Fe_{14}B$ phases were appeared. The peak intensities of the α-Fe, Fe_2Nb, Fe_3B, $Nd_2Fe_{23}B_3$ and $Nd_2Fe_{14}B$ phases at 760 °C were increased compared with the one annealed at 710 °C, indicating that the volume fractions of the each phase was slightly changed with increasing annealing temperature. The mean crystallite sizes for the α-Fe and $Nd_2Fe_{14}B$ phases at 760 °C were measured as 28.9 nm and 53.6 nm, respectively. This suggests that high temperature annealing treatment induces phase grain growth. The X-ray diffraction studies revealed that optimizing the annealing treatment for the $Nd_7Y_{2.5}Fe_{64.5}Nb_3B_{23}$ alloy is essential to fix the desirable volume fractions and crystallite sizes of the magnetic phases that, in turn, responsible to improve the magnet properties.

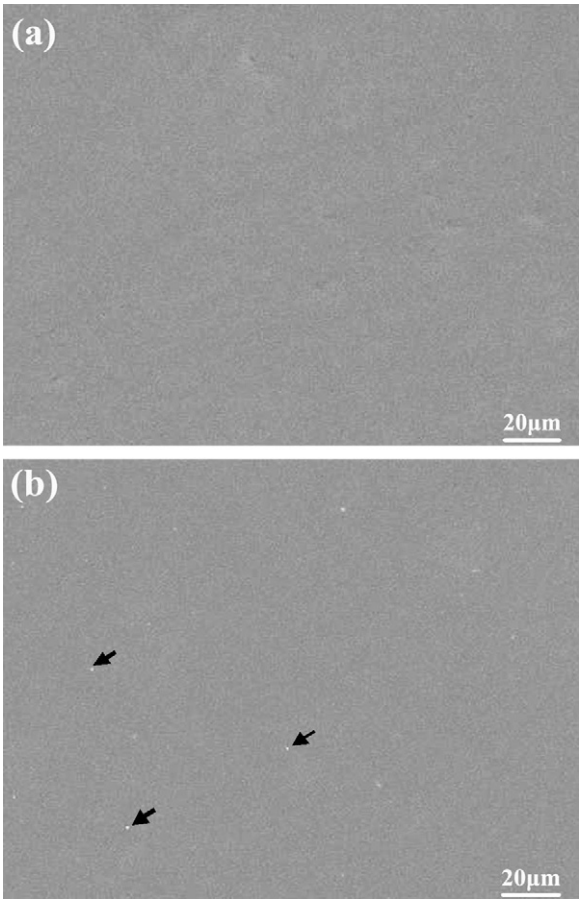

Fig. 3. HRSEM images showing (a) peripheral microstructure and (b) core microstructure of the as-cast rods.

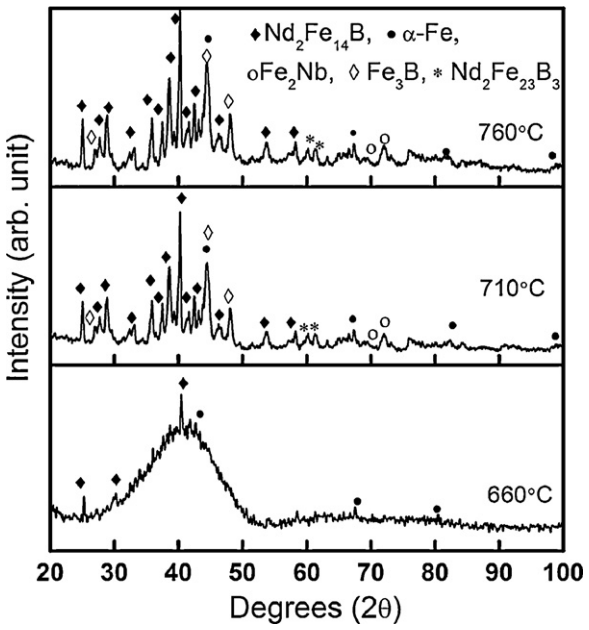

Fig. 4. X-ray diffraction patterns of the annealed magnets.

The HRTEM images of the optimally annealed magnets at 710 °C are presented in Fig. 5. Fig. 5a shows the dense distribution of the crystalline phase grains. The phases α-Fe, Fe_3B and $Nd_2Fe_{14}B$, detected in the microstructure were confirmed by the detail EDS analysis. The composition of the soft Fe_2Nb and $Nd_2Fe_{23}B_3$ magnetic phases was found to be difficult to determine due to overlapping of phase grains and indistinguishable images. The mean grain sizes for the soft α-Fe and Fe_3B phases were around 25 ± 5 nm and 28 ± 5 nm in diameter, respectively. The mean grain size for the hard $Nd_2Fe_{14}B$ phase was around 55 ± 10 nm in diameter. The high resolution feature for the α-Fe, Fe_3B and $Nd_2Fe_{14}B$ phase grains is depicted in Fig. 5b. It can be seen that the hard magnetic phase grain adjoin the soft magnetic phase grain, indicating the probability that exchange coupling exists between the soft and hard magnetic phases. Obviously, the smaller grains will result in larger contact area and increase the magnetic exchange coupling interactions that, in turn, enhances the magnetic performance of the magnets. The mean grain sizes measured with TEM was broadly in agreement with the X-ray measurements. The microstructural studies revealed that the annealed magnet microstructure contains nanoscale grains of the soft and hard magnetic phases whereby soft magnetic phase grain surrounded well to the adjacent hard phase grain with almost homogenous distribution in the composite microstructure.

The magnetization hysteresis loops for the as-cast and the magnets annealed at 660 °C, 710 °C, 760 °C and 810 °C for 15 min are presented in Fig. 6. The inset shows the magnetic hysteresis loop for the as-cast sample. The as-cast sample shows magnetically soft behavior which turns into magnetically hard due to nanocomposite microstructure induced by annealing the amorphous precursors. As seen in Fig. 6, the annealed magnets show the smooth hysteresis curves without steps, suggesting a strong exchange interaction between the soft and hard magnetic phases [29].

The magnetic properties of the annealed magnets are presented in Figs. 7 and 8. As seen, the sample treated at 660 °C exhibits coercivity ${}_jH_c$ of 120.5 kA/m, B_r of 0.29 T, $M_r/M_s = 0.52$ and BH_{max} of 9.6 kJ/m^3. At 660 °C, non-optimal volume content and grain size of

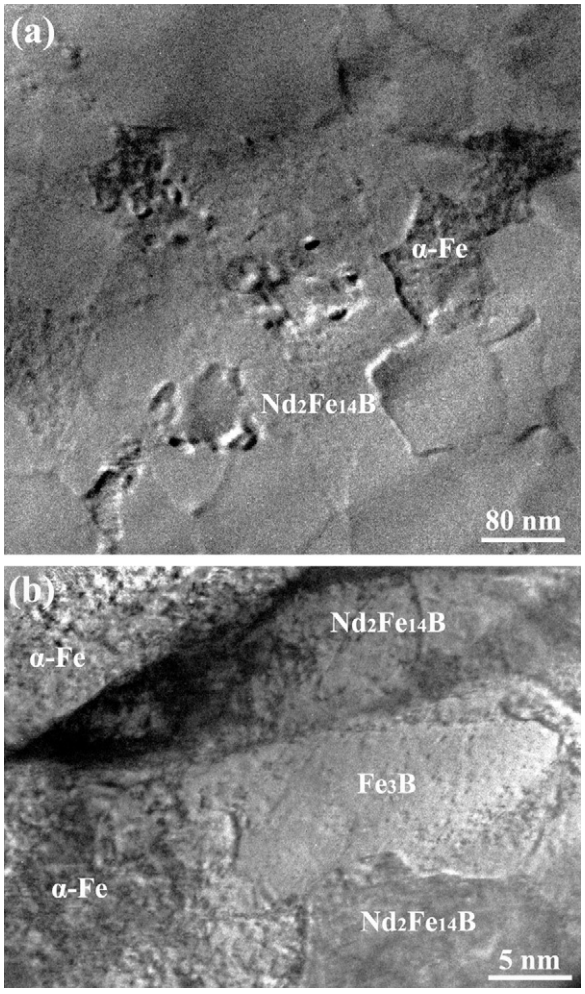

Fig. 5. HRTEM microstructures for the optimally annealed magnet showing (a) phase grains morphology and (b) a high resolution features of magnetic phase grains.

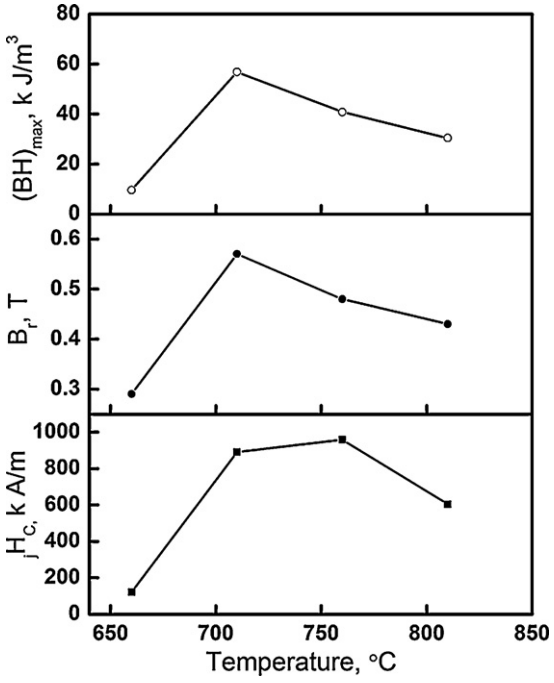

Fig. 7. Magnetic properties of thermally treated magnets.

magnetic phases cause the low magnetic properties. This is because some phase crystals do not grow fully due to incomplete crystallization. This suggests that high temperature annealing treatment is essential to improve the magnetic properties for the as-cast alloys. Annealing at 710 °C shows the magnetic properties such as $_jH_c$ of 891.52 kA/m, B_r of 0.57 T, M_r/M_s of 0.68 and $(BH)_{max}$ of 56.8 kJ/m^3.

The observed increase in B_r at 710 °C can be related to finer grain size (20–30 nm) of soft magnetic phases that tend to increase exchange coupling with the neighboring grains. Annealing at 760 °C leads to increase the coercivity from 891.52 kA/m to 959.18 kA/m at the expense of reduction in the remanence from 0.57 T to 0.46 T. The high coercivity at 760 °C may be related to optimal volume content and grain size of hard magnetic phase while coarsening of soft magnetic phases caused the reduction in remanence [29,30]. The annealing at 810 °C debases both $_jH_c$ and B_r drastically due to undesirable grain growth of the soft and hard magnetic

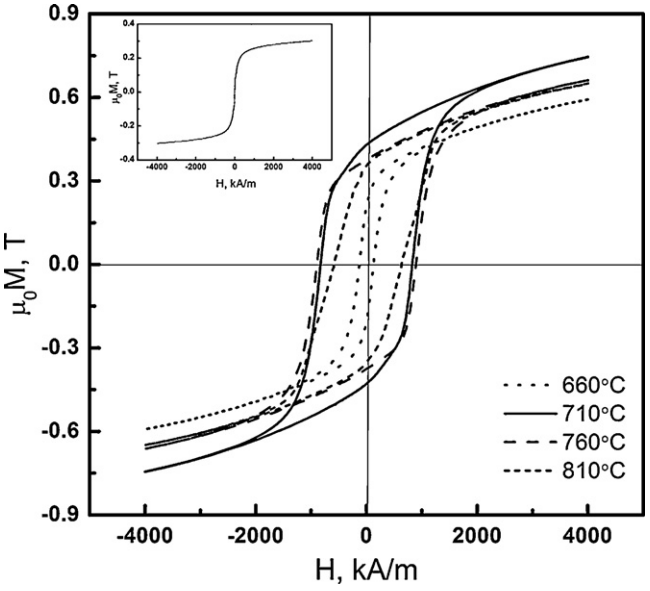

Fig. 6. Magnetic hysteresis loops of thermally treated magnets. The inset shows hysteresis loop of the as-cast rod.

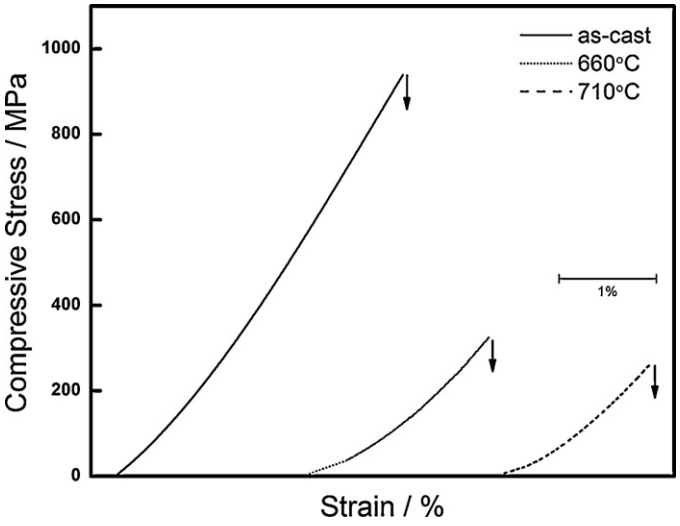

Fig. 8. Compressive true stress–strain curves for the as-cast and annealed rods with 2 mm in diameter.

Table 1
Mechanical properties of as-cast and annealed rods with 2 mm in diameter.

Condition	Hardness, H_v	Stress, MPa	Strain, %
As-cast	950 ± 20	894 ± 10	2.96
Annealed at 660 °C	1010 ± 20	309 ± 10	1.84
Annealed at 710 °C	1138 ± 20	239 ± 10	1.51

phases [31]. These results indicate that magnetic properties of the $Nd_7Y_{2.5}Fe_{64.5}Nb_3B_{23}$ magnets were affected by the intrinsic properties of the constituent phases. The magnetic properties of the $Nd_7Y_{2.5}Fe_{64.5}Nb_3B_{23}$ magnets can be further improved by controlling the elemental addition to the $Nd_7Y_{2.5}Fe_{64.5}Nb_3B_{23}$ alloys as well as by suppressing the metastable $Nd_2Fe_{23}B_3$ phase resulting in promoting large amount of $Nd_2Fe_{14}B$ and α-Fe phases with ultra fine grain size in the nanocomposite permanent magnets [32].

Fig. 6 compares the compressive stress–strain curves for the as-cast and annealed rods at 660 °C and 710 °C, respectively while the mechanical parameters are presented in Table 1. The as-cast rods show the mean compressive stress (σ_f) of 894 ± 10 MPa which decreased to 239 ± 10 MPa with increasing annealing temperature. The micro-Vickers hardness monotonically increases from H_v 950 ± 20 (as-cast rod) to H_v 1138 ± 20 (annealed rod at 710 °C). The behavior of the compressive stress and hardness can be related to the microstructure and crystalline structure of the $Nd_7Y_{2.5}Fe_{64.5}Nb_3B_{23}$ alloy. The as-cast microstructure comprised the amorphous phase along with a small amount of crystalline phase giving rise in the compressive stress value. The compressive stress decreases with the annealing temperature due to the precipitation of crystalline phases. In the annealed condition, magnets possess low symmetry of the crystalline structure, less slip plane system and complex microstructure, which contribute to the magnetic properties but are unfavorable to the mechanical properties [33–35]. The annealed microstructure contains $Nd_2Fe_{14}B$ hard magnetic phase grains (45–65 nm) and α-Fe, Fe_3B (20–30 nm) as the grain boundary phase (Fig. 5). Thus, when this magnet is loaded under the compressive stress testing, nucleation of microcracks might starts occurring at the grain boundary phase and once these appeared, they propagate along the grain boundaries, destroy the structure and caused the brittleness. This suggests that rapidly solidified nanocomposite permanent magnets are worst in brittle and toughness due its unique crystalline structure. Furthermore, the grain size, type and morphology of the grain boundary phase present in the microstructure can influence the magnetic and mechanical properties of the magnets. Grain boundary phase strengthening, defects controlling and wet-ability are the effective ways for the improvement of mechanical properties of the $Nd_2Fe_{14}B$ based permanent magnets [36,37].

The compressive strength and hardness of nanocomposite magnets can also be explained by the atomic bonding structure among the alloy constituents [38,39]. The atomic bonding structure is dictated by the atomic radius mismatch and enthalpies of mixing (ΔH^{mix}) values among the alloy constituents [40,41]. The large atomic size mismatch established a high packing density, whereby alloys with strong enthalpies of mixing lead to develop strong bonding structure. In the present alloy, the atomic radius of the alloy constituents is Fe 0.124 nm, Nb 0.143 nm, Nd 0.138 nm, Y 0.182 nm and B 0.09 nm [42]. The atomic radii of the elements decreases in the order of Y > Nb > Nd > Fe > B. These large differences in the atomic radii of the Y, Nb, Nd, Fe and B lead to improve the atomic packing density of the alloy. Moreover, the enthalpies of mixing (ΔH^{mix}) in the present alloy system for Fe–Y, Fe–Nb, Fe–B and Y–B atomic pairs is −54 kJ/mol, −42 kJ/mol, −49 kJ/mol, and −58 kJ/mol, respectively [43]. These negative enthalpies of mixing for the atomic pairs indicate a strong attractive interactions among the alloy constituent elements and leading to form atomic network structure known as backbone structure which, in turn, responsible to enhance the fracture strength of the present alloy system.

4. Conclusions

The $Nd_7Y_{2.5}Fe_{64.5}Nb_3B_{23}$ permanent magnets were produced in the form of rod with 2 mm in diameter by devitrification annealing of amorphous precursors produced by the simple copper mold casting. Annealing the as-cast rods at 710 °C for 15 min give a to best hard magnetic properties such as ${}_jH_c$ = 891.52 kA/m, M_r/M_s = 0.68, B_r = 0.57 T and $(BH)_{max}$ = 56.8 kJ/m^3. The homogeneity, fine grain sizes and ideal volume fractions of soft and hard magnetic phases present in the nanocomposite microstructure causes the high coercivity and remanence in the annealed magnets treated at 710 °C. The mechanical properties of the studied nanocomposite depend upon the sample composition as well as the processing parameters. The optimally annealed nanocomposite permanent magnet $Nd_7Y_{2.5}Fe_{64.5}Nb_3B_{23}$ exhibits the micro-Vickers hardness (H_v) of 1138 ± 20 and compressive stress (σ_f) of 239 ± 10 MPa. The present research work opens a new thought to develop nanocomposite magnets by substitution of nonmagnetic Y or La element for magnetic elements like Nd in $(Nd, Pr)_{3-9.5}–Fe_{bal}–M_{2-5}–B_{6-30}$; (M = Co, Mo, Nb, Ti, V, Zr) alloy systems.

Acknowledgments

This work was supported by the National Natural Science Foundation of China (Grant No. 50971113) and 863 program of China (No. 2009AA03Z112).

References

[1] A. Manaf, R.A. Buckley, H.A. Davies, J. Magn. Magn. Mater. 128 (1993) 302–306.
[2] R. Skomski, J.M.D. Coey, Phys. Rev. B 48 (1993) 15812.
[3] B.Y. Liang, Y.W. Xie, W. Li, W. Wu, X.Y. Zhang, J. Phys. D: Appl. Phys. 41 (2008) 195010.
[4] N.G. Akdogan, G.C. Hadjipanayis, D.J. Sellmyer, J. Appl. Phys. 105 (2009), 07A710.
[5] Y.G. Liu, L. Xu, Q.F. Wang, W. Li, X.Y. Zhang, Appl. Phys. Lett. 94 (2009) 172502.
[6] C.B. Rong, Y. Zhang, N. Poudya, X.Y. Xiong, M.J. Kramer, J.P. Liu, Appl. Phys. Lett. 96 (2010) 102513.
[7] H.W. Chang, M.F. Shih, C.C. Hsieh, W.C. Chang, C.Y. Shen, J. Alloys Compd. 489 (2010) 499.
[8] H.W. Chang, J.Y. Gan, C.C. Hsieh, X.G. Zhao, W.C. Chang, J. Appl. Phys. 107 (2010), 09A740.
[9] H. Jian, W. Luo, S. Tao, M. Yan, J. Alloys Compd. 505 (2010) 315–318.
[10] X.H. Tan, H. Xu, Q. Bai, W.J. Zhao, Y.D. Dong, Appl. Phys. Lett. 91 (2007) 252501.
[11] T. Schrefl, J. Fidler, H. Kronmüller, Phys. Rev. B 49 (1994) 6100.
[12] I. Betancourt, H.A. Davies, Mater. Sci. Technol. 26 (2010) 5–19.
[13] O. Gutfleisch, M.A. Willard, E. Brück, C.H. Chen, S.G. Sankar, J.P. Liu, Adv. Mater. 23 (2011) 821–842.
[14] D.C. Jiles, Acta Met. 51 (2003) 5907–5939.
[15] J.X. Zhang, I. Kleinschroth, Z.H. Cheng, D. Goll, H. Kronmüller, J. Appl. Phys. 86 (1999) 3274.
[16] D. Sultana, M. Marinescu, Y. Zhang, G.C. Hadjipanayis, Physica B 384 (2006) 306.
[17] J. Zhang, K.Y. Lim, Y.P. Feng, Y. Li, Scripta Mater. 56 (2007) 943–946.
[18] S.S. Hirosawa, H. Kanekiyo, T. Miyoshi, Y. Shioya, J. Magn. Magn. Mater. 239 (2004) 58–67.
[19] S. Tao, Z. Ahmad, H. Jian, T.Y. Ma, M. Yan, J. Alloys Compd. 509 (2011) 3843–3846.
[20] K. Hono, D.H. Ping, Mater. Sci. Eng. A 304–306 (2001) 81–87.
[21] S. Hirosawa, H. Kanekiyo, Y. Shigemoto, K. Murakami, T. Miyoshi, Y. Shioya, J. Magn. Magn. Mater. 239 (2002) 424–429.
[22] C. Zhian, L. Ji, S. Yanli, G. Zhimeng, J. Rare Earths 28 (2010) 277.
[23] W.H. Wang, Prog. Mater. Sci. 52 (2007) 540–596.
[24] T.D. Shen, R.B. Schwarz, Appl. Phys. Lett. 75 (1999) 5.
[25] A. Inoue, Mater. Trans. JIM 36 (1995) 866.
[26] D. Hanawalt, H.W. Rinn, L.K. Frevel, J. Ind. Eng. Chem. 10 (1938) 457.
[27] P. Scherrer, Gottinger Nachr. 26 (1918) 98.
[28] J. Zhang, H. Tan, Y.P. Feng, Y. Li, Scripta Mater. 53 (2005) 183–187.
[29] R. Fischer, H. Kronmuller, J. Appl. Phys. 83 (1998) 3271.
[30] Z.M. Chen, Y. Zhang, Y.Q. Ding, G.C. Hadjipanayis, Q. Chen, B.M. Ma, J. Magn. Magn. Mater. 195 (1999) 420.
[31] S.M. Parhofer, J. Wecker, C. Kuhrt, G. Gieres, L. Schultz, IEEE Trans. Magn. 32 (1996) 4437.

[32] H.W. Chang, C.C Hsieh, J.Y. Gan, Y.T. Cheng, M.F. Shih, W C Chang, J. Phys. D: Appl. Phys. 44 (2011) 064002.
[33] J.A. Horton, J.W. Herchenroeder, J.L. Wright, D.S. Easton, Mater. Trans. JIM 37 (1996) 860–863.
[34] Yu.M. Rabinovich, V.V. Sergeev, A.D. Maystrenko, V. Kulakovsky, Intermetallics 4. (1996) 641–645.
[35] W. Liu, J. Wu, J. Alloys Compd. 458 (2008) 292–296.
[36] H. Wang, A. Li, W. Li, Intermetallics 15 (2006) 985–988.
[37] Z.H. Hu, F.Z. Lian, M.G. Zhu, W. Li, J. Magn. Magn. Mater. 320 (2008) 2364–2367.
[38] C.Y. Lin, M.C. Lee, T.S. Chin, J. Phys. D: Appl. Phys. 40 (2007) 310.
[39] S.J. Poon, G.J. Shiflet, F.Q. Guo, V. Ponnambalam, J. Non-Cryst. Solids 317 (2003) 1–9.
[40] F.J. Liu, Q.W. Yang, S.J. Pang, T. Zhang, J. Non-Cryst. Solids 355 (2009) 1444.
[41] S. Tao, T. Ma, H. Jian, Z. Ahmad, H. Tong, M. Yan, Mater. Sci. Eng. A 528 (2010) 161–164.
[42] A. Takeuchi, A. Inoune, Mater. Trans. JIM 46 (2005) 2817.
[43] A. Takeuchi, A. Inoue, Mater. Trans. JIM 41 (2000) 1372.